

Machine Vision and Deep Learning Based Rubber Gasket Defect Detection

Chao-Ching Ho^{*}, Eugene Su, Po-Chieh Li, Matthew J. Bolger, Huan-Ning Pan

Graduate Institute of Manufacturing Technology and Department of Mechanical Engineering,
National Taipei University of Technology, Taipei, Taiwan

Received 17 May 2019; received in revised form 08 August 2019; accepted 18 October 2019

DOI: <https://doi.org/10.46604/aiti.2020.4278>

Abstract

This study develops an automated optical inspection system for silicone rubber gaskets using traditional rule-based and deep learning detection techniques. The specific object of interest is a 5 mm × 10 mm × 5 mm mobile device power supply connector gasket that provides protection against foreign body inclusion and water ingress. The proposed system can detect a total of five characteristic defects introduced during the mold-based manufacture process, which range from 10-100 μm. The deep learning detection strategies in this system employ convolutional neural networks (CNN) developed using the TensorFlow open-source library. Through both high dynamic range image capture and image generation techniques, accuracies of 100% and 97% are achieved for notch and residual glue defect predictions, respectively.

Keywords: traditional rule-based strategy, deep learning, convolutional neural networks (CNN), image recognition, image processing, deep residual learning

1. Introduction

Mobile device designers and manufacturers have made considerable efforts to increase the "ruggedness" of their products. One such effort has been the industry-wide adoption of the International Electromechanical Commission (IEC) published Inclusion Protection (IP) that rates electronic devices according to their protection against solid inclusion and water ingress. As mobile device components have become smaller and IP ratings higher, it has become necessary for manufacturers to be able to detect defects that are a few micrometers in size. Defect detection at this scale requires automated optical inspection techniques as traditional instrument-aided methods have been rendered obsolete.

The demand for silicone rubber-based components in the mobile device industry to provide tight seals to prevent foreign body inclusion and water ingress has been a boost for Taiwanese manufacturers. The strength of Taiwanese science and engineering has proved fundamental for the development and manufacture of natural and synthetic rubber products that require complex chemical refinement, bridging, and coloring sequences. Rubber mold manufacturing techniques can be broadly classified into three categories: sheet molding, injection molding, and extrusion molding, each of which introduces characteristic defects at varying rates and distributions.

As mobile device designers have decreased component size and increased ruggedness requirements, manufacturers have realized the necessity of automated optical inspection techniques for detecting defects a few micrometers in size. Furthermore, the non-invasive nature of optical inspection techniques provides the speed necessary for mass manufacturing.

In 1980, A. Cornforth and C. James proposed a rubber gasket inspection system to identify the void and lamination disband errors between the nylon tip and the rubber ring using an ultrasonic device [1]. Recently, systems have been developed for the prediction of silicone rubber solidification time through the optical measurement thickness [2]. Furthermore, optical

^{*} Corresponding author. E-mail address: HoChao@ntut.edu.tw

inspection-based systems to inspect the bubbles present in solid and liquid silicone rubber in the molding process have also been developed [3]. Machine vision measurement provides a non-invasive inspection process widely deployed in a broad range of smart manufacturing systems [4-6], e.g. leather production and manufacturing [7], leather defect-recognition [8], solenoid manufacturing [9], and in-process LED chip mounting alignment [10]. All the examples mentioned above feature dim and low reflective surface materials which make the proper illumination for defect detection difficult. In our previous study [11], we found that while machine vision-based systems are capable of defect classification performance, the performance of these systems was affected by variation in lighting conditions, and these systems were incapable of qualitative defect detection. Therefore, to ensure the homogeneity of the silicone rubber gaskets with its isolated components, a specified on-line measurement system for this application was developed in this study as shown in Fig. 1.

This study develops a fully automated optical inspection system for silicone rubber mobile device power supply connector gaskets. The defect detection application employs traditional rule-based and deep learning detection methods. Recently, several studies have been conducted on the application of deep learning methods for machine vision-based optical inspection systems [12-16].

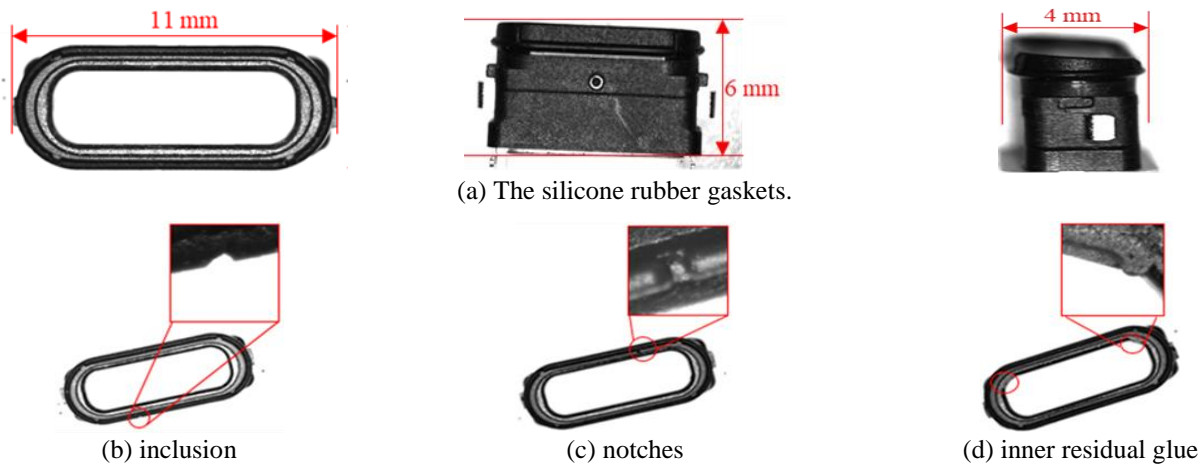


Fig. 1 Examined rubber gaskets



Fig. 2 Two types of side layer defects for the silicone rubber gaskets from side-view

2. Rule Based Image Detection Methodology

The mobile device power supply gasket inspection unit has two separate image capture stations, one is the top view and the other is the side view station as shown in Fig. 2. The top view station is used to examine three defects: outer ring inclusion, inner ring notches, and inner ring residual glue, whereas, the side view station checks for two defects: top edge inclusion and metal contact leg skewness.

2.1. Top-view station

The top view station captures the inspected object images using a Basler acA2500-14 μ m monochrome area scan industrial camera, fitted with a 50 mm CCTV lens. At the time of inspection, the camera was set to a $\times 0.343$ zoom for a 16×12 mm² sensor size and a precision of 6.4 μ m/pixel.

The top view station begins by acquiring multi-exposure images of the silicone rubber seal rings. The image processing application then creates both a contour approximation and a convex hull representation of the outer seal ring. As the eccentricity and straightness of the outer seal ring are rotation invariant, the application uses horizontal and vertical projections to segment the image. The application then calculates the difference in the segmented contour and convex hull representations to predict manufacturing defects as shown in Fig. 3. Because the top view optical inspection application does not use morphological operations or filtering, the image preserves the geometry of the inspected object at the pixel level. Thus, the application can correctly detect inclusion defects as small as 60 μm in size.

It is found that traditional rule-based image processing techniques are unable to accurately detect notch and inner residual glue defects because these defects are more qualitative in nature, thereby making them more suitable for deep-learning approaches.

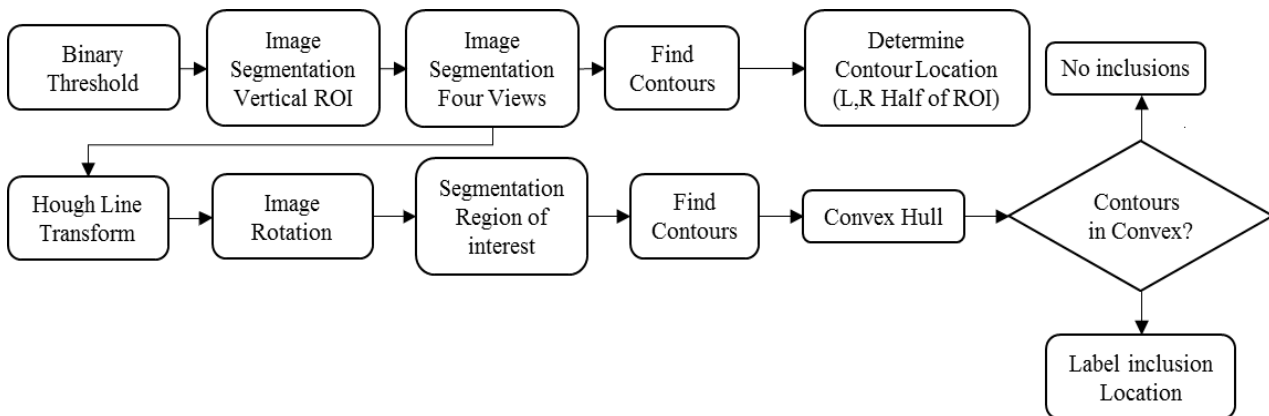


Fig. 3 Top view flowchart using traditional rule based image processing strategy

2.2. Side-view station

The second inspection station uses a Basler cA1600-20 μm monochrome area scan industrial camera equipped with an open four-view mirror to capture four side views. While the four-view mirror reduces the overall number of stations needed in the system, it increases the pre-processing time necessary to divide the distinct views as shown in Fig. 4. As illustrated in Fig. 5(a), the side view defect detection application first partitions the image using a predetermined region of interest (ROI). While this ROI attempts to consider most variations in the power supply gasket placement, excessively skewed or absent gaskets may lead to unpredictable results. The application uses a binary threshold to the ROI. The image processing application segments the image via horizontal projection techniques, which include additional parameters in the segmentation routine to control the magnitude of separation or overlap between the images as presented in Fig. 5(b). Additionally, a separate metal connection leg absence defect detection application is implemented using contour finding techniques. As shown in Fig. 6, the routine centroid calculations are allowed for the labeling of contour centroids to check for potential skew detection.

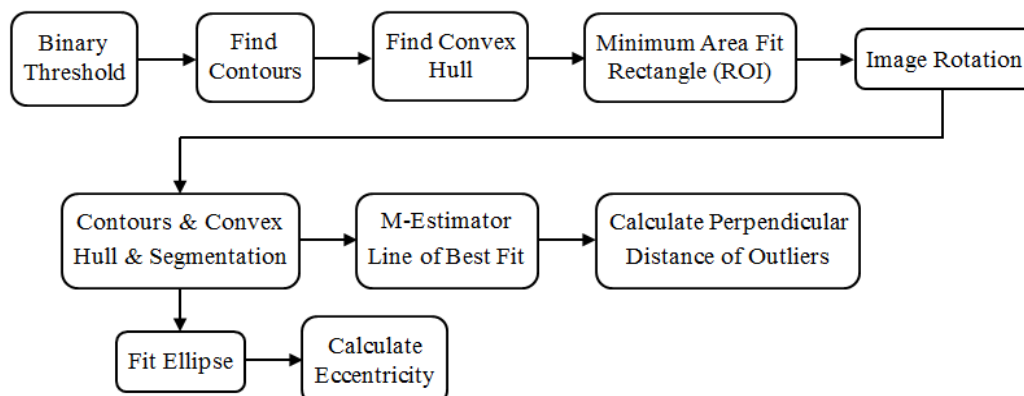


Fig. 4 Side view flowchart with using traditional rule-based strategy

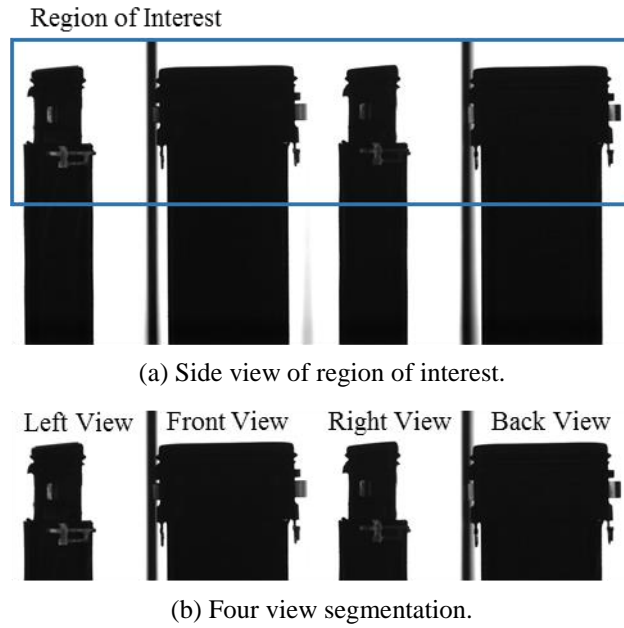


Fig. 5 Region of interest and image segmentation

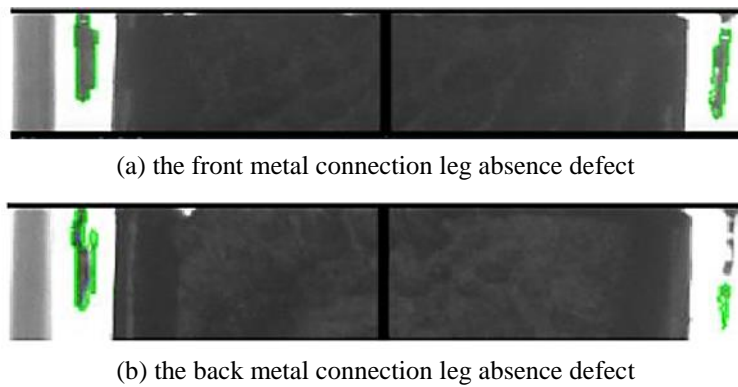


Fig. 6 Leg absence defect detection using contour finding techniques

The flow chart of top edge inclusion detection provides an intuitive explanation of the application logic. As the ROI is determined from the orientation of the top edge and subsequent affine transformation, the top edge defect detection allows improper placement of the power supply gasket on the fixture. The ROI is narrowed to account for the entire top edge and does not prevent errors that may arise when executing the inclusion finding a routine. The top edge material defects are observed by comparing the contour and convex hull representations of the top edge plastic material, as shown in Fig. 7.



Fig. 7 The detected top edge material defects

3. Deep Learning Approach

The top view defect detection application is improved by adding images and type labels to provide a labeling framework for potential machine learning applications. Therefore, quantitative information for more qualitative surface defects, namely inner ring notches and residual glue defects [17-18] were provided. To detect the surface type defects of the silicone rubber gaskets which have a rough and dim texture, a multi-exposure technique is used to enhance the illumination and highlight the defects. These multi-exposure images are then included in the dataset and trained in a 50-layer ResNet network [19-20]. The pixel size range of the defects is limited to avoid the feature vanishing during the convolution operations of the network and to

allow for more accurate discernment between the background and the defects. Moreover, the deep learning approach can indicate the defect types and defect positions within the predicted image.

3.1. Deep learning network structure

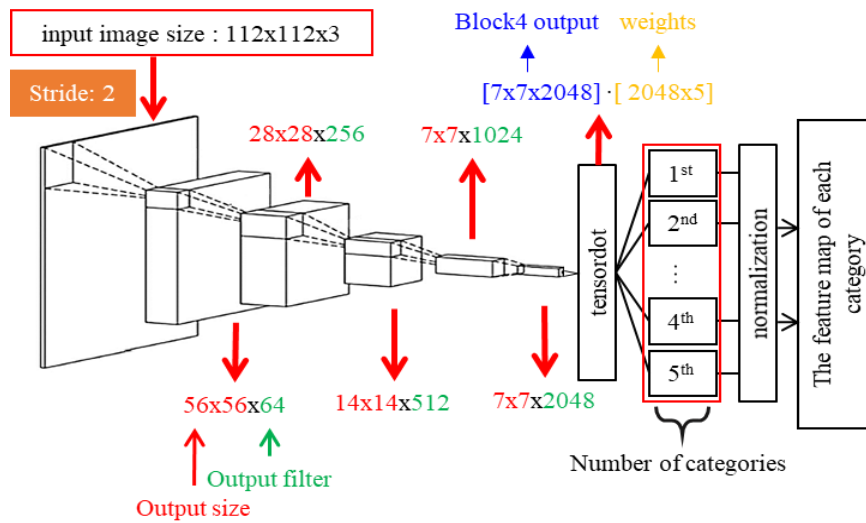


Fig. 8 The employed deep learning framework

Table 1 ResNet-50 structure

Layer name	Output size	ResNet 50-layer
Inputs	$224 \times 224 \times 3$	
conv1	$112 \times 112 \times 64$	$7 \times 7, 64, \text{stride } 2$
pool1	$56 \times 56 \times 64$	$3 \times 3 \text{ max pool, stride } 2$
conv2.x	$28 \times 28 \times 256$	$\begin{bmatrix} 1 \times 1, 64 \\ 3 \times 3, 64 \\ 1 \times 1, 256 \end{bmatrix} \times 3, \text{ stride } 2$
conv3.x	$14 \times 14 \times 512$	$\begin{bmatrix} 1 \times 1, 128 \\ 3 \times 3, 128 \\ 1 \times 1, 512 \end{bmatrix} \times 4, \text{ stride } 2$
conv4.x	$7 \times 7 \times 1024$	$\begin{bmatrix} 1 \times 1, 256 \\ 3 \times 3, 256 \\ 1 \times 1, 1024 \end{bmatrix} \times 6, \text{ stride } 2$
conv5.x	$7 \times 7 \times 2048$	$\begin{bmatrix} 1 \times 1, 512 \\ 3 \times 3, 512 \\ 1 \times 1, 2048 \end{bmatrix} \times 3, \text{ stride } 1$
pool5	1×2048	reduce mean
conv6	1×2	$1 \times 1, 1000, \text{stride } 1$

Table 2 RMPNet-50 structure

Layer name	Output size	ResNet 50-layer
Inputs	$112 \times 112 \times 3$	
conv1	$56 \times 56 \times 64$	$7 \times 7, 64, \text{stride } 2$
pool1	$56 \times 56 \times 64$	$3 \times 3 \text{ max pool, stride } 2$
conv2.x	$28 \times 28 \times 256$	$\begin{bmatrix} 1 \times 1, 64 \\ 3 \times 3, 64 \\ 1 \times 1, 256 \end{bmatrix} \times 3, \text{ stride } 2$
conv3.x	$14 \times 14 \times 512$	$\begin{bmatrix} 1 \times 1, 128 \\ 3 \times 3, 128 \\ 1 \times 1, 512 \end{bmatrix} \times 4, \text{ stride } 2$
conv4.x	$7 \times 7 \times 1024$	$\begin{bmatrix} 1 \times 1, 256 \\ 3 \times 3, 256 \\ 1 \times 1, 1024 \end{bmatrix} \times 6, \text{ stride } 2$
conv5.x	$7 \times 7 \times 2048$	$\begin{bmatrix} 1 \times 1, 512 \\ 3 \times 3, 512 \\ 1 \times 1, 2048 \end{bmatrix} \times 3, \text{ stride } 1$
pool5	1×2048	reduce mean
conv6	1×6	$1 \times 1, 6, \text{stride } 1$

ResNet is chosen as the deep residual network because its residual architecture effectively overcomes the vanishing gradient and explosion issues. As the ResNet in TensorFlow pre-training models and related high-level libraries are available in the open-source community, many comparative data for ResNet are available for industrial use. The network proposed in this paper uses a multi-class classifier constructed with ResNet 50-layer architecture. Part of the ResNet structure is modified by reducing the size of the receptive field, and the size of the feature map increased as shown in Tables (1)-(2), respectively. The proposed PMPNet network can be seen in Fig. 8. The size of the input picture of our proposed network was 112×112 pixels, and there is no max-pooling layer.

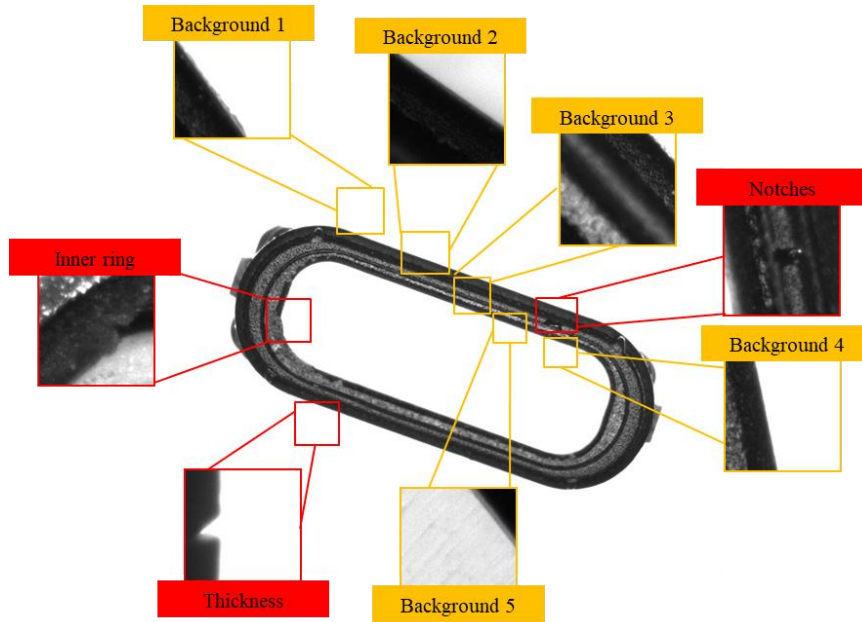


Fig. 9 The labelled defect types for deep learning

3.2. Training and dataset for deep learning network

The image of the surface defect and its annotation mask are labeled using the patch-based method. Fig. 9 shows the original image and the labeled defect types for deep learning. This work uses the TensorFlow open-source software library to develop a deep learning network and the corresponding training classifier. In addition to distinguishing the defects, this proposed method can also identify non-defective background images to increase detection accuracy. The training process is divided into two steps. The first step used the pre-trained model of ResNet V1 50-layers for transfer learning. It only trained for five epochs and updated the parameters of the last layer of the convolutional neural network layer. The parameters of the remaining network layers are fixed, the batch size was set to 64, the learning rate is set to 0.001, and the weight decay is set to 0.0004. The second step trained for 50 epochs and updated all network layer parameters, the batch size was set to 64, the learning rate is set to 0.0001, and the weight decay is set to 0.0004. The normalized exponential function is used as the basis of confidence for classifying in the last layer of the network. It is an extension of the Sigmoid function and can be termed as the Softmax function:

$$Softmax_j = \frac{e^{h_j}}{\sum_{j=0}^c e^{h_j}} \quad (1)$$

Furthermore, mean square error (MSE) is used to evaluate the loss function. MSE is expressed as:

$$MSE = \frac{1}{n} \sum_{i=1}^n (y_i - \hat{y}_i)^2 \quad (2)$$

In this study, a common data augmentation method such as mirroring and up and down flipping is used for image preprocessing.

3.3. Defect prediction for deep learning network

The cutting principle of defect detection is the same as the labeling dataset strategy, although the method and parameters were slightly different. The original large image is cut into several 112×112 segment patches in the stride of 64 and the trained defect classifier is used to predict the patches. The fused feature map of the defect category is normalized into a gray-scale map. As deep learning method requires a large amount of data to achieve accurate and efficient results. Each silicon rubber gaskets

is rotated by a mechanical turntable to acquire more image data from different lighting angles. The feature map corresponding to different colors according to different types of detected defects is shown in Fig. 10. During the prediction stage, the accuracies of the notch and residual glue defects were 97% and 80%, respectively. After rotating the objects under inspection at different angles, a series of images are obtained from different angles for the rubber gasket under evaluation. The collected images are analyzed for deep learning and the classification is chosen with voting. After voting, the prediction accuracies of the notch and residual glue defects were 100% and 97%, respectively. Compare to the traditional rule-based image detection approach, the deep learning approach has high classification performance. It can detect non-contour defects (i.e., notches and residual glue) and achieve valid prediction results.

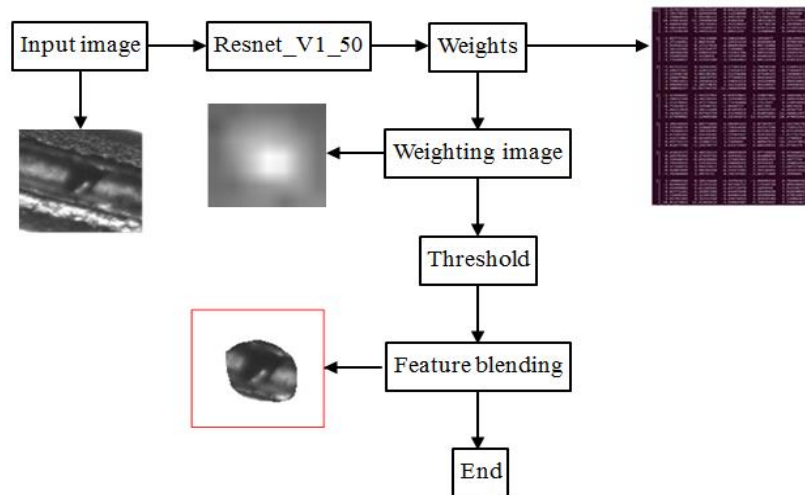


Fig. 10 The fused feature map after deep learning prediction

4. Conclusions

In this paper, defect detection for mobile device power supply connector gaskets using rule-based and deep learning image processing techniques is presented. Using a rules-based approach, outer ring inclusion and metal contact leg absence defects with 100% accuracy are successfully identified. The inner ring surface notch and residual glue defect detection applications are developed using deep learning approaches. Using the PMPNet framework, the overfitting phenomenon is avoided during all the proposed training steps, and the prediction accuracies of 100% and 97% are reached for the notch and residual glue defects, respectively. The high accuracy online inspection system for silicon rubber gaskets is implemented by fusing two different strategies successfully. Due to misjudgments caused by the instability of the light source, both approaches are desirable to help determine the stability of the light source processing before the light source correction mechanism. However, these two approaches require manual input to help to evaluate the value of the result. Further studies can be investigated to acquire feedback during the training process which will allow computers to make the decisions.

Acknowledgments

The authors would like to thank all of those reviewers who have provided helpful suggestions. We would also like to thank Pioneer Material Precision Technology for providing all the experiment samples.

Conflicts of Interest

The authors declare no conflict of interest.

References

- [1] A. Cornforth and C. James, "Ultrasonic system for the inspection of rubber gaskets," *NDT International*, vol. 13, no. 1, pp. 15-17, February 1980.

- [2] C. C. Kuo and Y. T. Siao, "Measuring the solidification time of silicone rubber using optical inspection technology," *Optik-International Journal for Light and Electron Optics*, vol. 125, no. 1, pp. 196-199, January 2014.
- [3] C. C. Kuo and Y. R. Chen, "Rapid optical inspection of bubbles in the silicone rubber," *International Journal for Light and Electron Optics*, vol. 124, no. 13, pp.1480-1485, July 2013.
- [4] R. Ciobanu, D. Rizescu, and C. Rizescu Ciprian, "Automatic sorting machine based on vision inspection," *International Journal of Modeling and Optimization*, vol. 7, no. 5, pp. 286-290, October 2017.
- [5] J. A. Marvel, R. Bostelman, and J. Falco, "Multi-robot assembly strategies and metrics," *ACM Computing Surveys*, vol. 51, no. 1, pp. 1-32, April 2018.
- [6] Y. X. Yang, Y. T. Lou, M. Y. Gao, and G. J. Ma, "An automatic aperture detection system for LED cup based on machine vision," *Multimedia Tools and Applications*, vol. 77, no. 18, pp. 23227-23244, September 2018.
- [7] C. C. Ho and T. R. Tsai, "Machine-vision-based servo control of a robotic sewing system," *Advanced Science Letters*, vol. 9, no. 1, pp. 45-49, April 2012.
- [8] C. C. Ho, J. C. Li, and T. H. Kuo, "Multicamera fusion-based leather defects marking system," *Advances in Mechanical Engineering*, vol. 5, 347921, January 2013.
- [9] C. C. Ho, Y. M. Chen, and T. Y. Chi, "Machine vision-based automatic placement system for solenoid housing," *Key Engineering Materials*, vol. 649, pp. 9-13, March 2015.
- [10] C. C. Ho, Y. M. Chen, and P. C. Li., "Machine vision based in-process LED chip mounting system," *Measurement and Control*, vol. 51, pp. 1-11, July 2018.
- [11] C. C. Ho and J. J. Liu, "Development of auto defect inspection system for cell phone silicone rubber gasket," *Proc. Tenth International Symposium on Precision Engineering Measurements and Instrumentation (ISPEMI 2018)*, SPIE Press, March 2019, pp. 1105303.
- [12] Y. J. Cha, W. Choi, and O. Büyüköztürk, "Autonomous structural visual inspection using region- based deep learning for detecting multiple damage types," *Computer- Aided Civil and Infrastructure Engineering*, vol. 33, no. 9, pp. 731-747, November 2017.
- [13] R. Ren, T. Hung, and K.C. Tan, "A generic deep-learning-based approach for automated surface inspection," *IEEE transactions on cybernetics*, vol. 48, no. 3, pp. 929-940, March 2018
- [14] Y. J. Cha, W. Choi, and O. Büyüköztürk, "Deep learning- based crack damage detection using convolutional neural networks," *Computer- Aided Civil and Infrastructure Engineering*, vol. 32, no. 5, pp. 361-378, March 2017.
- [15] G. S. Babu, P. L. Zhao, and X. L. Li, "Deep convolutional neural network based regression approach for estimation of remaining useful life," *Proc. International Conference on Database Systems for Advanced Applications (DASFAA)*, March 2017, pp. 214-228.
- [16] R. Ren, T. Hung, K.C. Tan, "A generic deep-learning-based approach for automated surface inspection," *IEEE Transactions on Cybernetics*, vol. 48, no. 3, pp. 929-940, March 2018.
- [17] G. Psuj, "Multi-sensor data integration using deep learning for characterization of defects in steel elements," *Sensors*, vol. 18, no. 1, January 2018.
- [18] X. C. Yang, H. Li , Y. T. Yu, X. C. Luo, T. Huang, and X. Yang, "Automatic pixel- level crack detection and measurement using fully convolutional network," *Computer- Aided Civil and Infrastructure Engineering*, vol. 33, no. 12, pp. 1090-1109, December 2018.
- [19] T. Wang, Y. Chen, M. Qiao, and H. Snoussi, "A fast and robust convolutional neural network-based defect detection model in product quality control," *The International Journal of Advanced Manufacturing Technology*, vol. 94, no. 9, pp. 3465-3471, February 2018.
- [20] R. F. Wei and Y. B. Bi, "Research on recognition technology of aluminum profile surface defects based on deep learning," *Materials*, vol. 12, no. 10, May 2019.



Copyright© by the authors. Licensee TAETI, Taiwan. This article is an open access article distributed under the terms and conditions of the Creative Commons Attribution (CC BY-NC) license (<https://creativecommons.org/licenses/by-nc/4.0/>).